Journal of Electronic Research and Application, 2026, Volume 10, Issue 8
http://ojs.bbwpublisher.com/index.php/JERA
Online ISSN: 2208-3510
Print ISSN: 2208-3502

Electrochemical Oxidation Dispersion of Graphene and Improvement of Its Compatibility with Coating Matrices

Qian Zhang*, Kaijie Yuan, Manjiao Deng, HailinWu

Grahope New Material Technology Inc., Shenzhen 518063, Guangdong, China

Corresponding author: Qian Zhang, zqsky2008@163.com

Abstract: The research employs a mild, controllable, and efficient electrochemical oxidation process using high-quality monolayer graphene powder prepared by a liquid-phase thermochemical route as the starting material. By optimizing key parameters including applied voltage and electrolyte concentration, a small number of hydrophilic oxygen-containing functional groups were selectively introduced at the edges of graphene, yielding a stably dispersed aqueous solution. The optimal conditions were determined as: graphene sheet anode, copper cathode, 0.4 mol/L NaOH electrolyte, voltage 8 V, and treatment time 30 min. Raman spectroscopy revealed an ID/IG ratio of 0.42. Thermogravimetric analysis and X-ray photoelectron spectroscopy confirmed that the oxygen content of electrochemically oxidized graphene (EGO) is low and that oxygen species are predominantly located at the edges; after reduction, the oxygen signals completely vanished, whereas residual oxygen remained in reduced GO. The as-prepared EGO aqueous dispersion achieved a concentration of 0.66 mg/mL and remained stable over six months of storage. TEM and AFM verified that the product retains a monolayer structure with an intact lattice. This approach preserves the intrinsic structure of graphene to the greatest extent while ensuring satisfactory dispersibility, thus offering a feasible pathway for fabricating high-performance graphene/siloxane ceramic resins and heavy-duty anti-corrosion coatings.

Keywords: Graphene; Electrochemical oxidation; Dispersion stability; Edge oxidation; Coating compatibility

Online publication: Sept 3, 2026

1. Introduction

Graphene, a two-dimensional carbon nanomaterial, possesses ultra-high specific surface area (2630 m^2/g), outstanding mechanical, electrical, thermal conductivity, and chemical stability [1]. It shows great potential in heavy-duty anti-corrosion coatings, composites, energy storage, etc [2,3]. Especially in anti-corrosion coatings, its lamellar structure blocks permeation of corrosive media (water, oxygen, chloride ions), and its conductivity suppresses electrochemical corrosion, making it an ideal functional filler [4–7]. However, two

major bottlenecks hinder practical use: (i) strong van der Waals forces (2.3 eV/nm^2) and large surface area cause agglomeration, preventing uniform dispersion; (ii) inert surface leads to poor interfacial compatibility with polar coating matrices (e.g., epoxy resins), and direct mixing causes phase separation [8,9].

To overcome these, various strategies have been explored [10,11]. Physical methods (high-speed shearing, ultrasonication) are simple but unstable and limited in concentration. Chemical modification introduces conjugated groups (phenyl, pyrenyl) to enhance π–π interaction. For instance, phenylbearing silane monomers stack onto graphene, then crosslink with silane coupling agents to improve matrix compatibility, but this requires stable concentrated aqueous dispersions.

Currently, two methods prepare aqueous dispersions: (1) direct ultrasonic or solventassisted exfoliation, simple but poor stability, low concentration (< 0.1 mg/mL), and reagglomeration; (2) Hummers method or modified, using strong oxidants to oxidize graphite to GO, then disperse in water, but this severely disrupts sp^2 conjugation, introduces many inplane defects, degrading electrical and mechanical properties irreparably [12]. Thus, a mild, controllable, efficient, and environmentally friendly method is urgently needed to ensure aqueous dispersibility while preserving pristine structure.

Recently, electrochemical oxidation has attracted attention due to mild conditions, controllable process, and selective modification [12–14]. Under an electric field, reactive oxygen species preferentially attack graphene edges, introducing limited oxygen groups (carboxyl, hydroxyl) to impart hydrophilicity without damaging the inplane lattice. In this study, highquality monolayer graphene powder prepared by a liquidphase thermochemical route was electrochemically oxidized. Effects of voltage and electrolyte concentration on structure, oxygen content, and dispersion stability were systematically investigated. Through a series of characterizations, the effectiveness and superiority of this strategy are demonstrated, providing a theoretical basis and technical support for graphene application in coatings.

2. Experiments

2.1. Materials and reagents

(1) Graphene powder

Self-prepared by a liquid-phase thermochemical method (graphitization at 3000 °C), confirmed by SEM, TEM, AFM, and particle size analysis to be large-size (ca. 7 μm), monolayer, and highly crystalline.

(2) N-methyl-2-pyrrolidone (NMP) and polyvinylidene fluoride (PVDF)

Analytical grade, commercially available.

(3) Sodium hydroxide (NaOH)

Analytical grade, for electrolyte preparation.

(4) Copper foil (purity ≥ 99.9%)

Used as cathode.

(5) Dialysis membrane (molecular weight cutoff: 1000 Da)

For product purification.

2.2. Preparation of EGO

The preparation involved five steps:

(1) Slurry preparation

Graphene powder and PVDF were mixed at a mass ratio of 10:1, and an appropriate amount of NMP

was added. The mixture was magnetically stirred at room temperature for 18 h to obtain a homogeneous slurry.

(2) Coating and drying

The slurry was coated onto a conductive substrate (e.g., titanium foil) by dip coating, followed by vacuum drying at 70–100 ℃ to obtain graphene sheet electrodes.

(3) Electrochemical oxidation treatment

The graphene sheet served as the anode, a copper foil as the cathode, and NaOH solution as the electrolyte. The treatment was conducted at a constant voltage for 30 min. Using the single-variable method, the effects of voltage (4, 6, 8, 10, 12 V, with fixed NaOH concentration of 0.4 mol/L) and electrolyte concentration (0.1, 0.2, 0.4, 0.6, 0.8 mol/L, with fixed voltage of 8 V) were investigated separately.

(4) Dialysis and concentration

The resulting solution was transferred into a dialysis bag and dialyzed against deionized water for 24 h to remove residual electrolytes and by-products, followed by concentration.

(5) Drying

Part of the concentrated solution was freeze-dried to obtain solid EGO powder for solid-state characterizations; the remaining liquid was kept for concentration and stability tests.

2.3. Characterization methods

The preparation involved five steps

(1) Raman spectroscopy

Performed on a confocal Raman spectrometer (excitation wavelength 532 nm) to analyze the positions and intensity ratios of D, G, and 2D bands for defect density evaluation.

(2) Thermogravimetric analysis (TGA)

Conducted under a nitrogen atmosphere from room temperature to 1000 ℃ at a heating rate of 5 ℃/min to determine the weight loss profile and estimate the content of oxygen-containing functional groups.

(3) Elemental analysis

Carried out using X-ray photoelectron spectroscopy (XPS) and energy-dispersive spectroscopy (EDS) to determine carbon/oxygen atomic percentages.

(4) Fourier-transform infrared spectroscopy (FTIR)

KBr pellet method, scanning range 400–4000 cm^{-1}.

(5) UV–visible spectroscopy (UV–vis)

Aqueous solutions, wavelength range 200–800 nm.

(6) Scanning electron microscopy (SEM) and transmission electron microscopy (TEM)

For morphology, lateral size, lattice observation; selected area electron diffraction (SAED) to verify crystal symmetry.

(7) Atomic force microscopy (AFM)

Tapping mode to measure thickness and evaluate lateral dimensions.

(8) Concentration determination

A known volume of EGO dispersion was freeze-dried, and the dry mass was weighed to calculate the mass concentration.

(9) Stability test

All samples were stored under identical ambient conditions for six months, and visual observation of sedimentation or stratification was recorded.

3. Results and discussion

3.1. Morphological characterization of the prepared graphene powder

The morphology and structure of the liquid-phase-derived graphene powder were characterized. TEM (**Figure 1**) showed large (micron-sized) transparent sheets, confirming their extreme thinness. HR-TEM (**Figure 2a**, **2b**) displayed a large-area (20 nm × 20 nm) defect-free hexagonal honeycomb lattice; the edge regions exhibited ultra-thin features, and the FFT pattern showed hexagonal symmetry, confirming single crystallinity. AFM (**Figure 3**) gave a thickness of about 0.6 nm, consistent with the theoretical thickness of monolayer graphene (ca. 0.34 nm, considering adsorbed layers). Particle size distribution (**Figure 4**) centered at approximately 7 μm, ranging from 1 to 30 μm. These results confirmed that the starting material is high-quality, large-size, monolayer graphene, providing an ideal substrate for subsequent electrochemical oxidation.

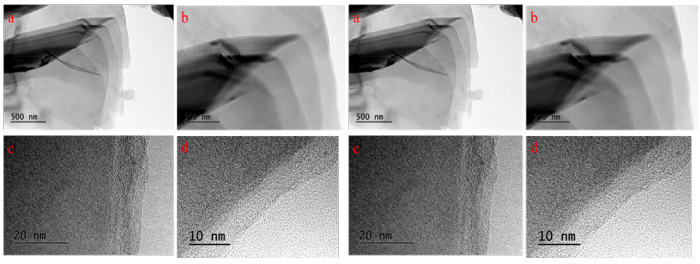

Figure 1. TEM image of a 3000℃ graphitized graphene.

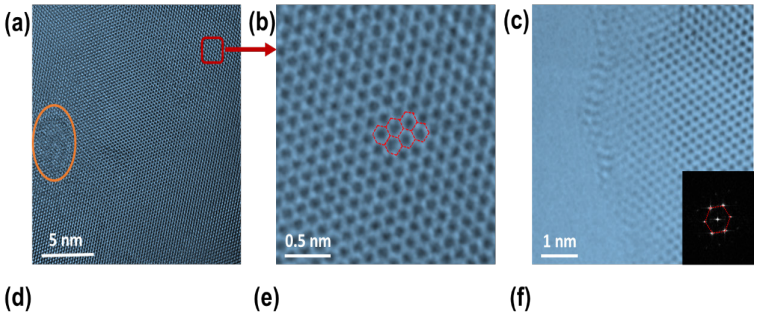

Figure 2. HR-TEM image of a 3000 ℃ graphitized graphene.

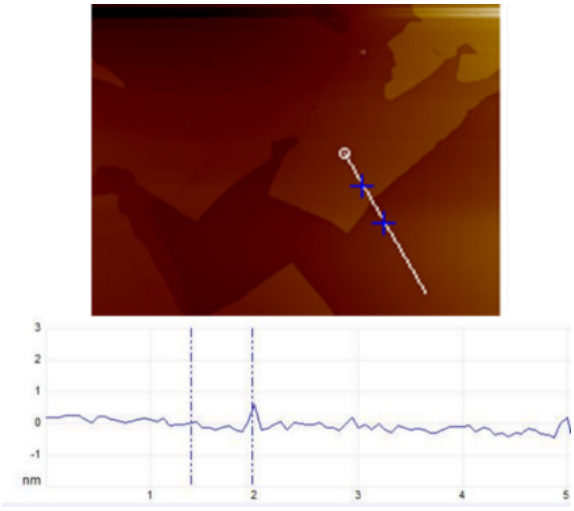

Figure 3. AFM image of a 3000 ℃ graphitized graphene.

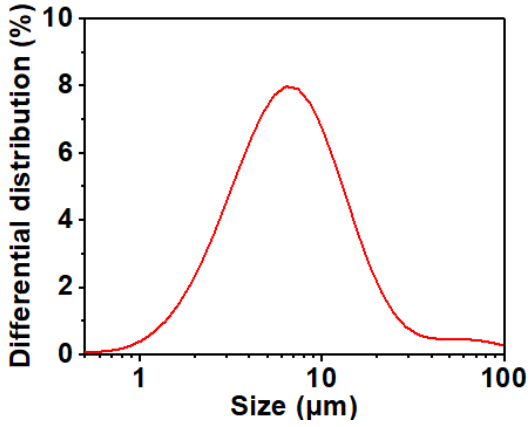

Figure 4. Particle size distribution of graphene powder.

3.2. Effect of voltage on EGO preparation

With a fixed NaOH concentration of 0.4 mol/L and treatment time of 30 min, the effect of applied voltage from 4 to 12 V was examined.

(1) Structural integrity (Raman)

As shown in **Figure 5** and **Table 1**, the D, G, and 2D band positions remained essentially unchanged (around 1350, 1580, and 2680 cm^{-1}) for all samples, indicating no significant chemical doping. However, with increasing voltage, the D-band intensity continuously increased, indicating more edge defects due to the introduction of hydrophilic groups. The G-band intensity first increased and then decreased, reaching a maximum at 8 V. The calculated ID/IG ratio reached its minimum (0.42) at 8 V, suggesting the fewest relative defects; the IG/I2D ratio was also smallest (0.67) at 8 V, indicating that the 2D band remained sharp and the lattice order was high. Therefore, 8 V was identified as the optimal voltage.

(2) Oxygen content (TGA and elemental analysis)

TGA (**Figure 6**) showed three-stage weight loss for all samples: < 200 ℃ (desorption of adsorbed water), 200–400 ℃ (decomposition of edge oxygen-containing groups), and > 400 ℃ (decomposition of more stable in-plane oxygen groups). With increasing voltage, the total weight loss increased, especially

above 8 V where the third-stage loss became pronounced, suggesting that oxygen groups penetrated the basal plane. Elemental analysis (**Figure 7**) further confirmed that as voltage rose from 4 V to 12 V, carbon content decreased from 98.89% to 64.52% and oxygen increased from 1.11% to 35.38%, with a sharp inflection at 8 V, indicating that 8 V is the threshold between selective edge oxidation and excessive bulk oxidation.

(3) Concentration and stability

Concentration measurements (**Figure 8**) showed that from 4 V to 8 V, the concentration jumped from 0.018 to 0.66 mg/mL, a dramatic increase; beyond 8 V, the increment became marginal (0.73 and 0.75 mg/mL). In terms of stability, samples at 4–8 V remained stable after six months, while the 10 V sample was "relatively stable" and the 12 V sample was unstable. Thus, 8 V yields the best compromise between good dispersibility and minimal oxidation.

Table 1. The ratio of peak intensity to peak height of EGO obtained under different voltages

	4V	6V	8V	10V	12V
D-peak intensity	188	523	868	1018	1427
G-peak intensity	270	490	2022	952	1269
2D-peak intensity	96	584	2996	139	188
I_D/T_G	0.69	1.06	0.42	1.06	1.12
I_G/T_{2D}	2.81	0.83	0.67	6.84	6.75

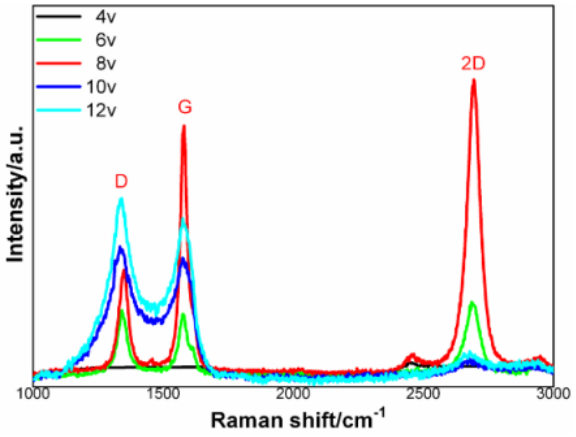

Figure 5. Raman spectra of EGO under different voltages.

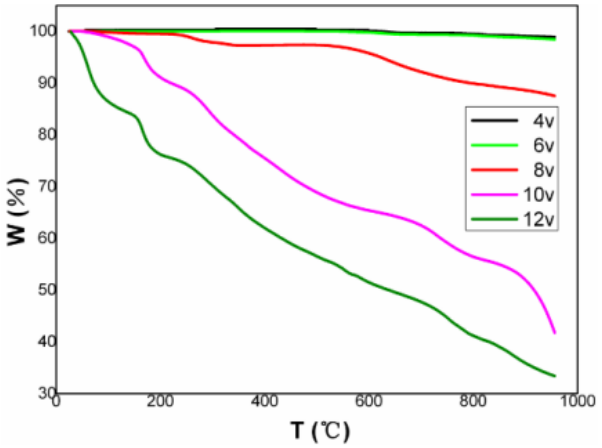

Figure 6. TGA of EGO under different voltages.

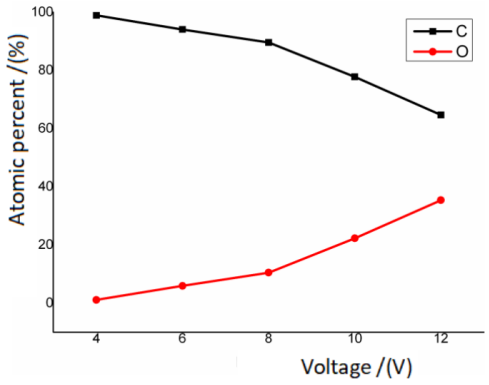

Figure 7. Carbon and oxygen element analysis of EGO under different voltages.

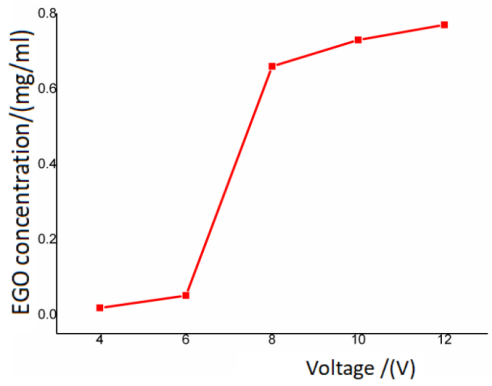

Figure 8. Concentration of EGO under different voltages.

3.3. Effect of electrolyte concentration on EGO preparation

With a fixed voltage of 8 V, NaOH concentrations from 0.1 to 0.8 mol/L were investigated.

(1) Structure (Raman)

Figure 9 and **Table 2** indicate that as concentration increased, the D-band intensity gradually rose; the ID/IG ratio at 0.4 mol/L was 0.73, slightly higher than 0.19 at 0.1 mol/L, but the latter showed a high IG/I2D of 2.37 (indicating significant broadening of the 2D band). Overall, the 2D band remained sharp at 0.4 mol/L, and the degree of defects was acceptable. In general, the influence of electrolyte concentration on structure was weaker than that of voltage.

(2) Oxygen content (TGA and elemental analysis)

TGA (**Figure 10**) also exhibited three-stage weight loss, but the loss increased more gently with concentration, and no further loss occurred above 600 °C. Elemental analysis (**Figure 11**) showed oxygen content increasing from 7.03% at 0.1 mol/L to 18.63% at 0.8 mol/L, without abrupt changes, indicating a gradual effect, with overall oxidation levels much lower than those at high voltage (35.38% at 12 V).

(3) Concentration and stability

Concentration data (**Figure 12**) indicated that at 0.4 mol/L the concentration reached 0.67 mg/mL, after which it nearly saturated (0.72–0.74 mg/mL). Samples at 0.4 mol/L and below were stable; 0.6 mol/L was "relatively stable", and 0.8 mol/L was unstable. Considering all factors, 0.4 mol/L was chosen as the optimal electrolyte concentration.

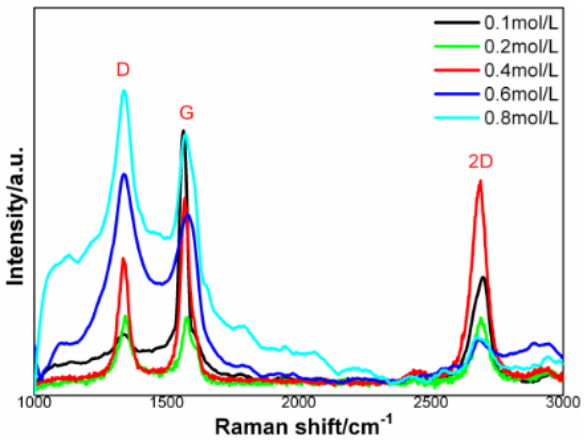

Figure 9. Raman spectra of EGO under different electrolyte concentrations.

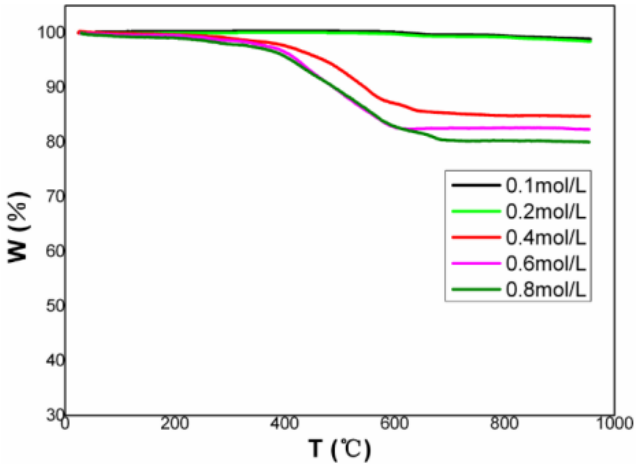

Figure 10. TGA of EGO under different electrolyte concentrations.

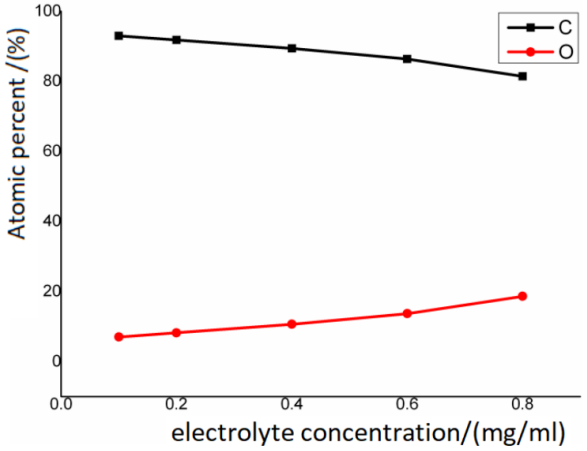

Figure 11. Carbon and oxygen element analysis of EGO under different electrolyte concentrations.

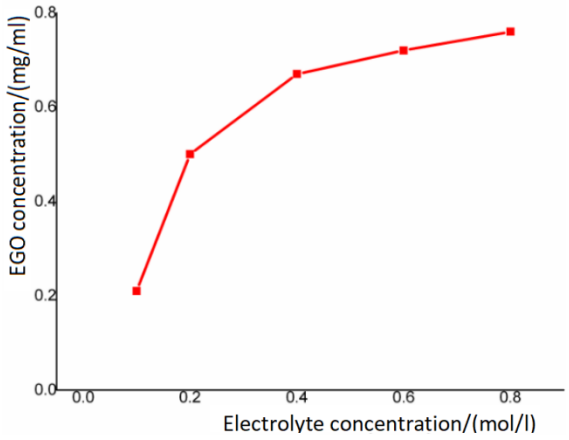

Figure 12. Concentration of EGO under different electrolyte concentrations.

Table 2. The ratio of peak intensity to peak height of EGO obtained under different electrolyte concentrations

	0.1 mol/L	0.2 mol/L	0.4 mol/L	0.6 mol/L	0.8 mol/L
D-peak intensity	386	506	986	1661	2322
G-peak intensity	1993	512	1446	1344	1988
2D-peak intensity	839	521	1817	349	366
I_D/T_G	0.19	0.98	0.73	1.23	1.16
I_G/T_{2D}	2.37	0.98	0.79	3.85	5.43

3.4. Study on EGO structure under optimal conditions

Under the optimal conditions (8 V, 0.4 mol/L NaOH), EGO was prepared, and the structural morphology was characterized.

(1) TEM (**Figure 13**)

EGO appeared as thin, loose sheets with enlarged interlayer spacing due to edge hydrophilic groups. TEM confirmed that EGO remained transparent and thin, with clear lattice fringes; SAED exhibited a six-fold symmetric diffraction pattern, confirming monolayer structure and intact crystallinity.

(2) AFM (**Figure 14**)

The thickness of EGO was 0.7–1.2 nm, falling within the typical range for monolayer oxidized graphene (considering group and water adsorption), confirming the monolayer nature.

(3) XPS comparison (**Figure 15**)

Before reduction, the C/O atomic ratio of EGO was significantly higher than that of GO, indicating lower oxidation. After reduction, the O 1s signal completely vanished for rEGO, whereas a residual O signal remained for rGO, demonstrating that the in-plane oxygen groups of GO are difficult to remove fully, while the edge groups of EGO are readily reducible. This further verifies the minimal damage and good reversibility of the electrochemical oxidation approach.

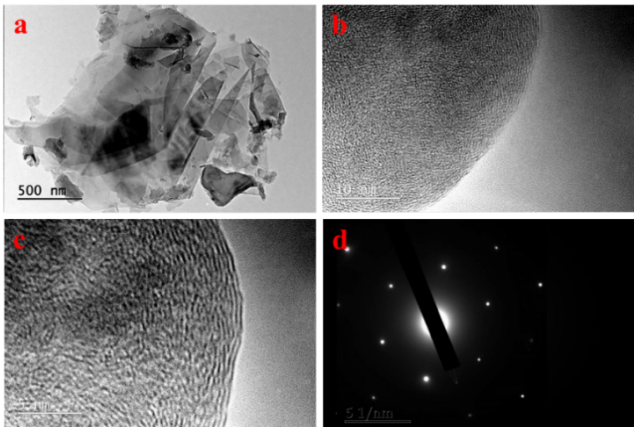

Figure 13. TEM image of EGO and its selected area electron diffraction pattern.

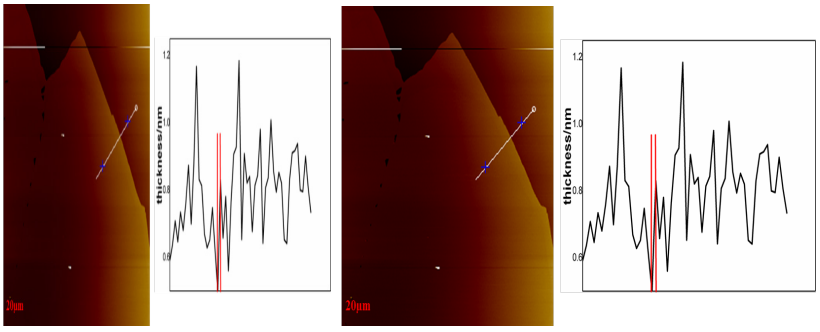

Figure 14. AFM image of EGO.

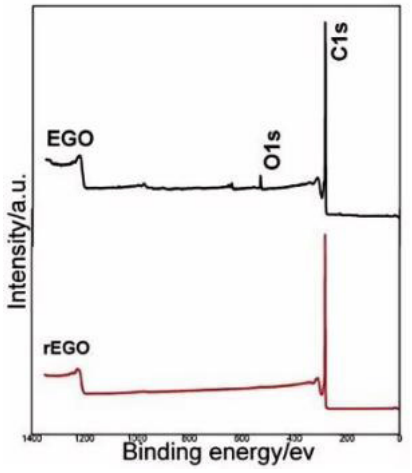

Figure 15. XPS spectra of EGO and rEGO.

4. Discussion

Collectively, the mechanism of electrochemical oxidation can be rationalized as follows: under the applied electric field, OH^- and reactive oxygen species in the aqueous solution preferentially attack the carbon atoms at the edges of graphene (due to their higher reactivity), generating carboxyl, hydroxyl, and other hydrophilic groups, while the in-plane hexagonal rings, being more energetically stable and kinetically hindered, are

less susceptible to oxidation. Moderate oxidation (8 V, 0.4 mol/L) introduces sufficient groups to provide hydration-layer electrostatic repulsion (increased Zeta potential) for stable dispersion, while avoiding in-plane defects. When voltage or electrolyte concentration exceeds the optimum, the oxidation intensifies, and groups extend into the basal plane, leading to lattice deterioration and reduced stability. Compared with the Hummers method, the electrochemical route avoids strong acids and oxidants, operates under mild conditions, and allows precise control of oxidation degree via electrical parameters, thus representing a green and controllable strategy.

The EGO dispersion prepared by this method achieves a concentration of 0.66 mg/mL, far exceeding that of ultrasonication-based methods (typically < 0.1 mg/mL), with excellent stability. More importantly, the preserved intact lattice ensures that the electrical conductivity and mechanical properties of graphene are retained, which is beneficial for subsequent grafting of phenyl-containing silane molecules via π–π stacking to improve compatibility with coating matrices, thereby providing high-quality feedstock for the fabrication of high-performance graphene/siloxane ceramic resin anticorrosion coatings.

5. Conclusion

(1) Using large-size (ca.7 μm), monolayer, highly crystalline graphene powder prepared by a liquid-phase thermochemical route as the starting material, an electrochemical oxidation method was employed to selectively introduce hydrophilic oxygen-containing functional groups (hydroxyl, carboxyl) at the edges of graphene, successfully yielding a stably dispersed aqueous graphene dispersion and overcoming the obstacle of graphene agglomeration in water.

(2) Through systematic optimization, the optimal preparation conditions were determined as: graphene sheet anode, copper cathode, 0.4 mol/L NaOH electrolyte, voltage 8 V, and treatment time 30 min. The resulting EGO dispersion reached a concentration of 0.66 mg/mL and remained stable without sedimentation for six months.

(3) Multi-dimensional characterizations (Raman, TGA, elemental analysis, XPS) demonstrated that the oxidation degree of EGO is much lower, with an ID/IG ratio of only 0.42, oxygen species predominantly located at the edges, and an intact in-plane lattice. EGO preserves the intrinsic structure of graphene to the greatest extent while ensuring satisfactory dispersibility.

(4) The electrochemical oxidation method is mild, controllable, and pollution-free. It offers a new route for the scalable application of graphene in waterborne coatings and composite materials.

Acknowledgments

Industrial Foundation Strengthening Project Shenzhen Key Industry R&D Plan

Funding

Industrial Foundation Strengthening Project Shenzhen Key Industry R&D Plan (Project No.: JSGG20200925145800001)

Disclosure statement

The authors declare no conflict of interest.

References

[1] Geim A, Novoselov K, 2007, The Rise of Graphene. Nature Materials, 6(3): 183–191.

[2] Guo X, Qing F, Li X, 2021, Applications of Graphene in Anti-Corrosion of Metal Surface. Acta Physica Sinica, 70(9): 098102.

[3] Zhang Y, Sun J, Xiao X, et al., 2022, Graphene-Like Two-Dimensional Nanosheets-Based Anticorrosive Coatings: A Review. Journal of Materials Science & Technology, 129: 139–162.

[4] Wang P, Cai D, 2020, Preparation of Graphene-Modified Anticorrosion Coating and Study on Its Corrosion Resistance Mechanism. International Journal of Photoenergy, 2020: 1–9.

[5] Daradmare S, Raj S, Bhattacharyya A, et al., 2018, Factors Affecting Barrier Performance of Composite Anti-Corrosion Coatings Prepared by Using Electrochemically Exfoliated Few-Layer Graphene as Filler. Composites Part B, 155: 1–10.

[6] Li T, Zhan H, Lan H, et al., 2023, Graphene Oxide Modification and Its Application in Anticorrosive Epoxy Coatings. Journal of Chemical Engineering of Chinese Universities, 37(4): 525–536.

[7] Wang B, Cunning B, Ruo R, et al., 2016, Graphene Coatings as Barrier Layers to Prevent the Water-Induced Corrosion of Silicate Glass. ACS Nano, 10(11): 9794–9800.

[8] Yue X, Zhang X, Qiao Y, et al., 2025, A Review on Properties of Graphene Modified Thermosetting Resin Matrix Composites. Materials Reports, 39(9): 240401771–9.

[9] Govindaraj P, Sokolova A, Salim N, et al., 2021, Distribution States of Graphene in Polymer Nanocomposites: A Review. Composites Part B: Engineering, 226: 109353.

[10] Georgakilas V, Tiwari J, Kemp K, et al., 2016, Noncovalent Functionalization of Graphene and Graphene Oxide for Energy Materials, Biosensing, Catalytic, and Biomedical Applications. Chemical Reviews, 116(9): 5464–5519.

[11] Qamar S, Ramzan N, Aleem W, 2024, Graphene Dispersion, Functionalization Techniques and Applications: A Review. Synthetic Metals, 307: 117697.

[12] Pei S, Wei Q, Huang K, et al., 2018, Green Synthesis of Graphene Oxide by Seconds Timescale Water Electrolytic Oxidation. Nature Communications, 9: 145.

[13] Yang S, Lohe M, Mullen K, et al., 2016, New-Generation Graphene From Electrochemical Approaches: Production and Applications. Advanced Materials, 28(29): 6213–6221.

[14] Hao S, Hou S, Liu Y, et al., 2025, Enhanced Anticorrosion of Waterborne Epoxy Coatings by Electrochemical Exfoliated Graphene Oxide. Progress in Organic Coatings, 202: 109147.